Korean J. Chem. Eng., 40(8), 1871-1881 (2023)
DOI: 10.1007/s11814-023-1513-0

pISSN: 0256-1115
eISSN: 1975-7220

Rheological and molecular dynamics simulation studies of the gelation of human serum albumin in anionic and cationic surfactants

Tochukwu Olunna Nnyigide, Osita Sunday Nnyigide, and Kyu Hyun†

School of Chemical Engineering, Pusan National University, Busan 46241, Korea
(*Received 23 April 2023 • Revised 12 June 2023 • Accepted 14 June 2023*)

Abstract−We report the gelation of human serum albumin (HSA) of 5-12 wt% concentrations in 0-0.15 M aqueous solutions of a cationic surfactant, cetyltrimethylammonium bromide (CTAB), or an anionic surfactant, sodium dodecyl sulfate (SDS), under isothermal and nonisothermal conditions. Under both conditions, the initial increase in the CTAB concentration (up to 0.075 M) accelerated HSA gelation (marked by decreasing gel times (t_{gel}) for the isothermal case or gel temperature (T_{gel}) for the nonisothermal case), whereas increasing the SDS concentration inhibited HSA gelation (i.e., increasing t_{gel} or T_{gel}). The increase and decrease in HSA gelation by CTAB and SDS, respectively, reached a maximum at a surfactant/protein molar ratio of 100. Rheological properties, i.e., storage modulus (G′) and loss modulus (G″), exhibited mechanically stable behavior of HSA/CTAB gels over the covered concentration range, whereas HSA/SDS gels exhibited decreasing mechanical properties with increasing SDS concentration. Molecular dynamics simulation showed that the greater rate of the unfolding of the HSA structure in CTAB than in SDS was behind the rapid gelation kinetics of HSA in CTAB compared with SDS. Our result establishes that cationic CTAB and anionic SDS surfactants exert wide-ranging control over the rheological and kinetic properties of HSA hydrogels.

Keywords: Human Serum Albumin (HSA), Hydrogel, Rheology, Sodium Dodecyl Sulfate (SDS), Cetyltrimethylammonium Bromide (CTAB)

INTRODUCTION

Human serum albumin (HSA) is an important transport protein and drug binder that constitutes approximately 66% of human blood plasma [1,2]. Research interest in albumins has continued to rise due to their utilization in the fabrication of biodegradable, biocompatible, and bioactive hydrogels with medical and pharmaceutical applications [3-5].

Owing to rapidly evolving use cases requiring hydrogels with unique viscoelastic properties, the need to develop methods for tuning hydrogels for desired characteristics has become evident [6,7]. For instance, while hydrogels to be used as organ scaffolds in tissue engineering need to have sufficient mechanical properties to support their target organs, hydrogels used in targeted-organ drug delivery are typically expected to have shear-thinning properties to enable them to flow easily under the push of the syringe but solidify upon entry into an organ target, thereby restricting them to the target organ [8,9]. Therefore, to induce tunable hydrogel properties, various additives such as denaturants, salts, and sugars have been explored [10].

Although various experimental techniques for studying hydrogels exist [11], the rheological measurement method stands out because it is not limited by the concentration regime of samples. Moreover, rheological measurements are sensitive to the microstructure of materials [12] and thus can chronicle structural changes associated with the transition of gelling species, such as proteins from the solution to the gel state [9,13-16]. For example, temperature ramp and time sweep tests conducted within the linear viscoelastic region of a protein solution could reveal the onset of aggregation following the unfolding of the protein, thereby offering information about the activation energies and rates associated with the gelation process [15]. To characterize the sol–gel transition behavior and mechanical property of hydrogels, researchers typically employ rheological measurements, performed under small material deformations [3,9]. A common small deformation measurement typically employed for this purpose is the small amplitude oscillatory shear (SAOS) test. Due to the small deformation, i.e., the linear viscoelastic regime, the SAOS method has the advantage of being a nondestructive measure of material functions [17]. It is very useful for characterizing a variety of complex fluids [18,19].

The growth of material functions during sol-gel transitions under isothermal and nonisothermal conditions exhibits features such as those of n^{th}-order chemical reaction kinetics. Based on this analogy, the reaction kinetic equation developed by Rhim [20] has been rewritten in terms of measurable material functions G′ or G″ for calculating the reaction rates and activation energies during sol-gel transitions. Following this method, the associated reaction order and activation energies during the gelation of several gelling species, including bovine serum albumin (BSA), BSA/cetyltrimethylammonium bromide (CTAB), and BSA/sodium dodecyl sulfate (SDS) complexes, have been established [10,21,22]. For protein systems, such kinetic data are useful for pharmaceutical drug development, protein replacement in food applications, and an in-depth understanding of the protein gelation process [10,23-25].

†To whom correspondence should be addressed.
E-mail: kyuhyun@pusan.ac.kr

Although several protein hydrogel systems have been investigated, studies comparing the gelation of HSA in an anionic or a cationic solution (e.g., SDS and CTAB surfactants) and that links structural unfolding, aggregation processes, and rheological properties are scarcely reported. Hence, in this study, we compared the rheological properties of HSA under increasing concentrations of CTAB or SDS. To understand this process, we analyzed the gel temperature (T_{gel}) from a rheological temperature ramp test and the gel time (t_{gel}) obtained via a rheological time sweep test at a fixed temperature (above T_{gel}). The denaturing effects of the surfactants as well as a molecular level understanding of protein aggregation in the presence of the surfactants were investigated by molecular dynamics (MD) simulation.

MATERIALS AND METHODS

1. Preparation of HSA Solution

HSA, CTAB, SDS, and phosphate-buffered saline (PBS) were purchased from Sigma-Aldrich (USA) and used without modification. All samples were prepared at room temperature (25 °C). PBS diluted ten times with distilled water was used as the solvent, with PBS acting to keep the pH condition near neutral (pH ~7.6). HSA/surfactant aqueous solutions were prepared with HSA concentrations of 5, 7, 10, and 12 wt%, containing CTAB or SDS concentrations of 0-0.15 M (Tables 1 and 2). The prepared solutions were stirred for 1 h at room temperature before use.

2. Rheological Measurements

All rheological measurements were performed using a stress-controlled rheometer (Discovery HR 20, TA instruments, USA) with a 40 mm diameter parallel plate and stainless-steel Peltier plate. The exposed edges of the samples were covered with silicone oil to mitigate evaporation. To determine thermal gelation properties, a temperature ramp test was conducted at 25-90 °C, 1 rad/s angular frequency, and 0.05 strain amplitude. Time sweep tests were conducted at a constant temperature of 80 °C for HSA/surfactants containing 10 and 12 wt% HSA. Higher HSA concentrations were used in the time sweep test because the rapid heating and protective effect of SDS prevented the gelation of HSA below 10 wt% within the surfactant concentrations measured.

Table 1. Concentrations of HSA, CTAB, and SDS in the temperature ramp experiment

HSA [wt%]	CTAB/SDS concentration [M]
5, 7, 10	0.000
	0.008
	0.038
	0.075
	0.150

Table 2. Concentrations of HSA, CTAB, and SDS in time sweep experiment and molecular dynamics simulation

HSA [wt%]	CTAB/SDS concentration [M]		Mol ratio
	Experiment	Simulation	
10, 12	0.000	0.00	0
	0.008	0.01	5
	0.038	0.05	25
	0.075	0.20	100
	0.150	0.30	150

3. Molecular Dynamics Simulation

MD simulations of HSA were performed using GROMACS 2018.7 and the methods already in use [10,26-28]. The structure of HSA was obtained from the RCSB protein data bank [29,30]. All simulations were performed at 80 °C, the same temperature as the experiments conducted under the isothermal time sweep test. The protein was solved using the N*p*T (constant number of particles (N), pressure (*p*) and temperature (T)) ensemble and a cubic box with dimensions of 11.182×11.182×11.182 nm, as depicted in Fig. S1 of Supporting Information. HSA was simulated in a cubic box containing 0, 0.01, 0.05, 0.1, and 0.2 M CTAB or SDS. The amount of HSA and surfactant in the box corresponds to HSA surfactant ratios of 0, 10, 50, 100, and 200 (see supporting document Table S3), which are approximately equal to the average protein/surfactant molar ratios used in the experiment. The correspondence between experimental and simulated concentrations allows a comparison between the dynamic properties from simulation and gelation properties obtained by rheology. The GROMOS 53A6 force field and a simple point charge water model were used in all simulations, and all simulations were performed for 150 ns in a cubic box [31]. Prior to the production run, each system was energy minimized based on the steepest decent algorithm, and subsequently, NVT (constant number of particles (N), box volume (V) and temperature (T)) and N*p*T ensemble equilibration runs, each lasting 2 ns, were performed to relax the system before the production run.

RESULTS AND DISCUSSION

1. Temperature Ramp Testing of HSA/CTAB and HSA/SDS Solutions

Temperature ramping from 25 °C to 90 °C or 25 °C to 100 °C was used to explore the nonisothermal gelation characteristics of HSA/CTAB and HSA/SDS solutions, respectively. In this method, the temperature was increased at a constant rate of 0.5 °C/min, whereas a small strain amplitude (=0.05) and angular frequency (1 rad/s), within the linear viscoelastic regime, was used to measure the viscoelastic properties (i.e., storage modulus G′ and loss modulus G″) of the sample, which were then used to characterize sol-gel transition properties. The same conditions were used in all the temperature ramp measurements [10,12,32]. The thermal gelation of various proteins proceeds in parallel with distinct structural evolution for globular proteins [10,39], as illustrated in Fig. 1. Generally, proteins in their native state exist in type-specific three-dimensional (3D) folded shape, known as their tertiary structure, upon which their functionality depends (left panel, Fig. 1). In this state, charged and polar residues of proteins are exposed to the protein surface, whereas hydrophobic residues tend to reside deep within the structure. In water, exposed charged and polar residues on the protein surface interact with water molecules, enabling protein solvation. Typically, protein functionality is lost when proteins are

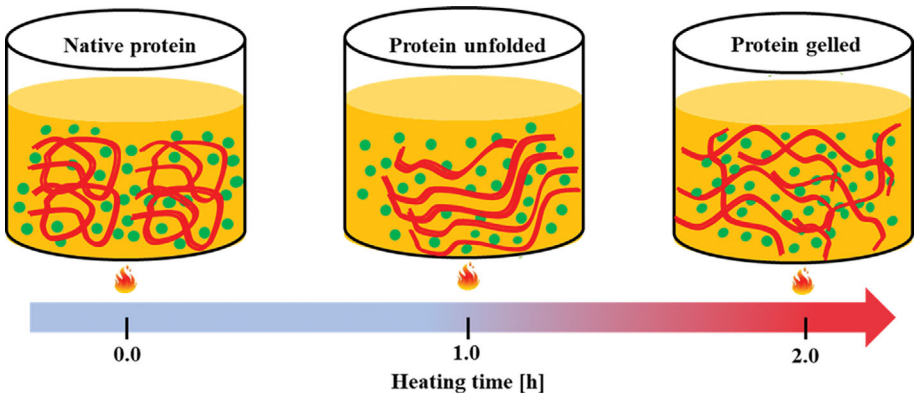

Fig. 1. Simplified illustration of various conformations of aqueous proteins undergoing sol-gel transition: (left) native-folded protein molecules, (middle) unfolded protein cluster at a short heating time or low temperature, and (right) percolated network of joined clusters. The green dots represent co-solvents, salts, or denaturants, and the yellow surface, along with proteins, constitutes a solution.

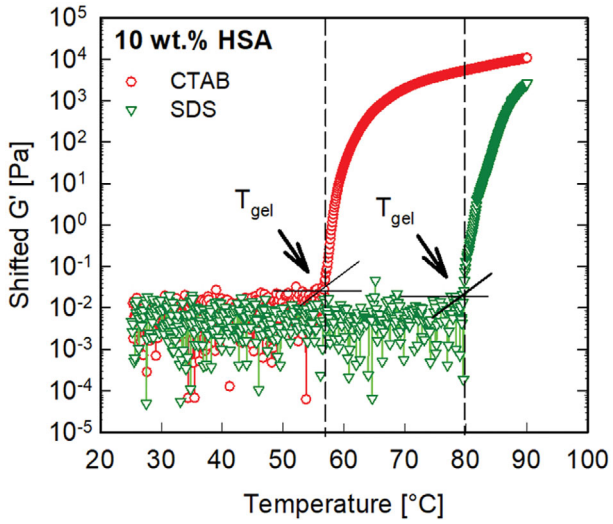

Fig. 2. Typical gelation curve for 10 wt% HSA with CTAB or SDS of concentration of 0.038 M. The arrow points to the T_{gel} determined as the point at which G′ deviates from the baseline.

unfolded (middle panel, Fig. 1) [33-37]. Thus, when aqueous proteins are exposed to high thermal energy, changes in pH, or the presence of chemical denaturants, the balance of attractive and repulsive interactions between protein molecules may be altered, resulting in the unfolding of their secondary and tertiary structures, protein aggregation, and the possible formation of a percolated gel network (right panel, Fig. 1) [10,37-40].

Typical gelation of the HSA/surfactant solution is depicted in Fig. 2, with the rest shown in Supporting Information (Fig. S2(a)-(f)). Fig. 2 shows that the storage modulus (G′) of the HSA/CTAB solutions did not vary over the temperature range of 25-50 °C. This period is characterized by weak and temperature-independent viscoelastic properties that correspond to the solution state (illustrated in Fig. 1, left panel). As shown in Fig. S2, this behavior varied with the CTAB concentrations and between the two surfactants (i.e., CTAB compared with SDS). However, as the temperature increased further up to 55 °C (Fig. 2), G′ increased as a function of temperature, indicating the onset of denaturation and gelation or a space-spanning percolated network of dimensions within the bulk. Above the denaturation temperature, the number of unfolded protein molecules increased with time [38-41], and G′ increased as more native proteins unfolded and were converted to aggregates. Overall, the evolution rate of G′ depends on the rate of unfolding and the presence of bond restructuring within protein aggregates [11,39,42].

Based on the literature, the temperature at which the storage modulus (G′) equaled the loss modulus (G″) and began to rapidly evolve, indicating a shift toward more elastic or solid-like behavior, was taken as the gelation temperature T_{gel}, i.e., the temperature T at which G′=G″ [43,44]. According to the temperature ramp results, HSA mixed with various concentrations of either CTAB or SDS exhibited varied sol-gel transition behavior, as evidenced by variation in T_{gel} and the increase in the storage modulus post-gel temperature.

The variation in T_{gel} with concentration of either surfactant for 5, 7, and 10 wt% HSA has been calculated and plotted in Fig. 3. The T_{gel} of the HSA/CTAB solutions decreased significantly with the addition of low concentration (0.008-0.038 M) of CTAB compared with pure HSA. This suggests that a small amount of CTAB disrupts the structural stability of HSA in aqueous solutions, resulting in the occurrence of faster protein unfolding and aggregation at temperature below the standard denaturation temperature of HSA. Detailed retention of pure HSA helical structures in solutions at various temperatures may be found in other literature, such as Moriyama [45]. The reduced T_{gel} of the HSA/CTAB solutions is presumed to be due to the more destabilizing interaction between HSA and CTAB. T_{gel} reached a minimum value of 50 °C, 57.5 °C, and 59 °C for 5, 7, and 10 wt% HSA, respectively, at a 0.038 M surfactant concentration. However, at higher concentration (>0.038 M of CTAB), T_{gel} began to increase. In contrast, the addition of low SDS concentration (0.008-0.038 M) of SDS increased the gelation temperature of the HSA/SDS solutions beyond that of pure HSA. T_{gel} reached a maximum at a 0.075 M SDS concentration. This suggests that low SDS concentration shields HSA from thermal gelation. This result agrees with other recent reports, suggesting that the addition of a small amount of SDS to HSA confers enhanced structural stability to HSA molecules and prevents helicity loss for

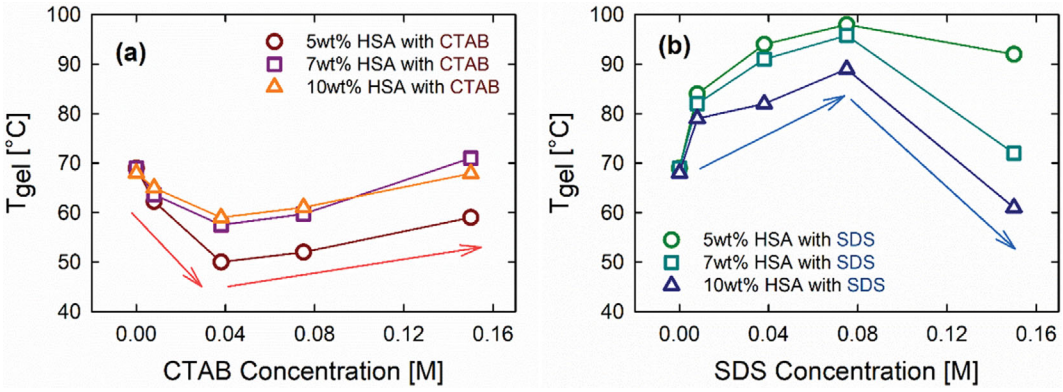

Fig. 3. Variation in gel temperature (T_{gel}) of 5, 7, and 10 wt% HSA, with (a) CTAB and (b) SDS as a function of concentration.

up to 80 °C [45]. However, the trend reverses at higher SDS concentration (>0.075 M of SDS), as the T_{gel} of HSA/SDS drops toward that of pure HSA, signaling the weakening of the protective effect of SDS on HSA. T_{gel} values remained lower than that of pure HSA for 5, 7, and 10 wt% HSA with CTAB concentration of up to 0.075 M. The T_{gel} values of HSA with SDS were higher than those of HSA with CTAB in the same concentration range, indicating that CTAB comparatively decreases the T_{gel} of HSA, whereas SDS increases it.

The effect of HSA concentration was monitored using 5, 7, and 10 wt% HSA with surfactant concentration of 0-0.150 M. It was found that with increasing HSA concentration, T_{gel} increased for HSA/CTAB solutions. This may be due to the increase in the repulsive interaction, which contributes to the stability of aqueous globular proteins. As the protein concentration increases (which may be likened to decreasing CTAB to HSA molar ratios), a decreasing number of CTAB molecules would bind to single protein molecules. If the number of bound CTAB molecules is just insufficient to create more neutral HSA/CTAB complexes, the net charge of these complexes would determine the strength of the long-range repulsion that keeps the complexes apart. Therefore, reduced binding could yield more repulsive HSA/CTAB complexes; conversely, sufficient binding would shift the absolute net charge of HSA/CTAB complexes toward neutral, thereby reducing the strength of the stabilizing long-range electrostatic interaction. The reduction in the repulsive interaction strength is expected to lower the energy cost of aggregation, thereby lowering the gelation temperature. Conversely, T_{gel} decreased with increasing protein concentration for the HSA/SDS solutions, and this is presumed to be due to an increase in protein-protein interactions with increasing HSA concentration.

The net charges of proteins are dependent on pH, and it is well known that their repulsive effects play a crucial role in maintaining the separation of protein molecules (i.e., prevent aggregation and gelation) [15,45,46]. For HSA, Fogh-Andersen [46] reported an overall net charge of −24 at pH 7.6. If all surfactant molecules were to be considered bound to the protein molecule, the net charge per protein molecule can be calculated by considering the amount and net charges of the species present i.e., HSA (−24), CTAB (+1) and SDS (−1). A lower absolute net charge would therefore suggest a lower repulsion (gelation acceleration), whereas a higher absolute net charge would indicate higher repulsion (gelation inhibition) [38,39]. However, calculated net charges achieve higher accuracy in predicting protein behavior at low surfactant concentration regimes in which surfactant-surfactant interaction is not significant [47]. The calculated average net charge per HSA molecule in CTAB and SDS is shown in Tables S4 and S5 of the supporting information. As Table S4 shows, adding a small amount of CTAB reduces the absolute net charge of HSA until a trend reversal occurs at or near 0.038 M. Higher HSA concentration has a higher absolute net charge, which agrees with the effect of HSA on T_{gel} observed in Fig. 3(a). Unlike in CTAB, where the absolute net charge decreased before increasing, the absolute net charge increased monotonically with increasing SDS concentration, signaling an increase in repulsion or gelation hindrance from onset. Additionally, the absolute net charge of HSA in SDS varied inversely with HSA concentration. This agrees with the variation of T_{gel} in SDS shown in Fig. 3(b).

2. Nonisothermal Modeling of HSA/CTAB and HSA/SDS Gelation

Gelation proceeds with the denaturation and aggregation of protein molecules separated ab initio. The elastic modulus G′, which shows the solution-gel transformation process, increases as denatured proteins become aggregates, and subsequently, the gel network reaches a plateau when no more proteins are joining the network [37,48-50]. An increase in G′ can be treated as an analog of a chemical reaction in which reactants are converted into products; in this case, non-aggregated aqueous protein molecules (reactants) are converted into aggregates and later cross-linked proteins in a 3D space-spanning network. The diffusion of protein chains through the solution has been suggested as the main phenomenon controlling the nature of the resultant gel fractals according to the reaction kinetic model. If the bond-making processes are faster than the diffusion processes, such a reaction is called diffusion limited, whereas the opposite case is termed reaction limited. The gelation of globular proteins is mostly reaction limited aggregation [15, 39,48].

If the concentration of non-aggregated proteins is denoted by C_{na}, the change in the concentration of nonaggregated proteins with time is as follows:

$$\frac{dC_{na}}{dt} = -KC_{na}^{n}, \quad (1)$$

where n is the reaction order, and K is the rate constant. The reac-

tion order provides information about the dependency of the reaction rate on the concentration of the reacting species, which in this case represents non-aggregated proteins [38].

The rate constant K is well represented by the Arrhenius model:

$$K = K_o e^{\frac{-E_a}{RT}}, \quad (2)$$

where E_a is the activation energy, K_o, R, and T are pre-exponential factor, universal gas constant and absolute temperature respectively.

Integrating (1) and combining the result with (2) yields the following:

$$\ln\left[\frac{d}{dt}\left(\frac{C_{na}^{1-n} - C^{1-n}}{1-n}\right)\right] = \ln K_o - \left(\frac{E_a}{R}\right)\left(\frac{1}{T}\right) \quad (3)$$

C is the lower limit of C_{na} from integration of (1).

However, although G′ increases as most of the native proteins become aggregates, no clear universal relationship between G′ and the gel microstructure has been found; thus, the left-hand side of (3) is not well known.

By combining the reaction kinetic rate equation of (1) and linear temperature increase, Rhim [20] developed a nonisothermal model of (3) for reactions occurring under linearly increasing temperatures. da Silva [51] later adapted the equation for application to nonisothermal gelation kinetics by replacing concentration with the material function G′.

$$\ln\left(\frac{1}{G'^n}\frac{dG'}{dt}\right) = \ln K_o - \left(\frac{E_a}{R}\right)\left(\frac{1}{T}\right) \quad (4)$$

For 7 and 10 wt% HSA, regression analysis based on (4) was performed to obtain the kinetic parameters as a function of CTAB and SDS concentrations. All kinetics followed first-order kinetics (i.e., reaction order n=1), with the best fit R^2=0.91. A similar reaction order has been reported for various protein gelling systems, and other reaction orders such as 1.5 and 2 have also been reported [10,39].

The variation in the activation energy with CTAB or SDS concentration obtained from the regression analysis is shown in Fig. 4. The gelation activation energy of 13.6 kJ/mol was found for 10 wt% HSA containing no surfactant. The predicted value was within the range of activation energy reported for proteins of similar properties [33]. The addition of surfactants, i.e., CTAB and SDS, has opposite effects on the activation energy, with CTAB addition leading to a decrease, whereas SDS addition increasing the estimated activation energy. Decreasing T_{gel} for HSA/CTAB solutions corresponds with lowering gelation activation energy, whereas the increase in T_{gel} observed in HSA/SDS is consistent with the activation energy observed in SDS.

3. Isothermal Gelation Kinetics of HSA/CTAB and HSA/SDS

The gelation behavior of HSA/CTAB and HSA/SDS solutions was tested under isothermal conditions by holding the samples at a constant temperature above or close to their T_{gel} while measuring their rheological properties. A temperature of 80 °C was employed in all isothermal measurements because it is above the maximum gel temperature of HSA/CTAB solutions and close to the maximum gel temperature of HSA/SDS with a 10 wt% HSA concentration and thus results in a high probability of gelation in all concentrations tested. Due to the high gel temperatures observed in HSA/SDS solutions with HSA concentrations of <10 wt%, 10 and 12 wt% HSA samples were used for the time sweep testing. A typical gelation curve of the 10 wt% sample containing 0.150 M SDS is shown in Fig. 5(a). Initially, the elastic modulus (G′) has low and widely fluctuating values because the rheological properties of the solution state are low and near the rheometer's resolution limits. However, after some time intervals, G′ values increase until reaching a plateau due to the onset of gelation. For HSA/CTAB solutions, G′ values evolve rapidly with little or no lag and increase until reaching the plateau. The gelation of the HSA/SDS solutions was more delayed with a rapid rise in G′ only seen at an SDS concentration of 0.008 M, for both 10 and 12 wt% HSA (see Supporting Information Fig. S3). Beyond 0.008 M SDS, a significant lag phase is observed before the onset of gelation (i.e., a rapid increase in G′). The lag phase here describes the period before gelation when the G′ value is very low and does not vary with time [11]. Generally, the HSA/CTAB solutions exhibited faster gelation kinetics than the HSA/SDS solutions. The rapid rise in the G′ of HSA/CTAB agrees with the rapid gelation observed for HSA/CTAB in the temperature ramp test. Overall, both the isothermal and nonisothermal results agree, with both suggesting that CTAB destabilizes the structure of HSA at low surfactant concentrations, resulting in rapid denaturation and gelation kinetics, whereas SDS plays a stabilizing role at the same concentration regime, resulting in slower denaturation and gelation kinetics. Visually, HSA/CTAB gels are more opaque

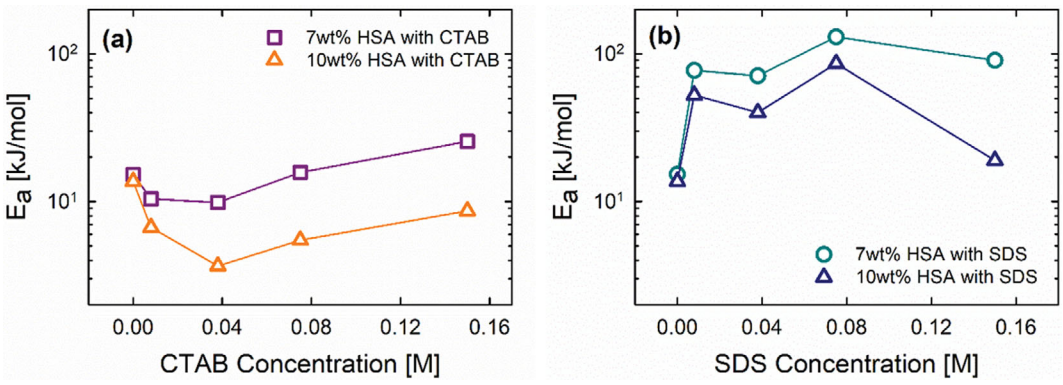

Fig. 4. Variation in activation energy of 7 and 10 wt% HSA with 0-0.15 M concentrations of (a) CTAB and (b) SDS.

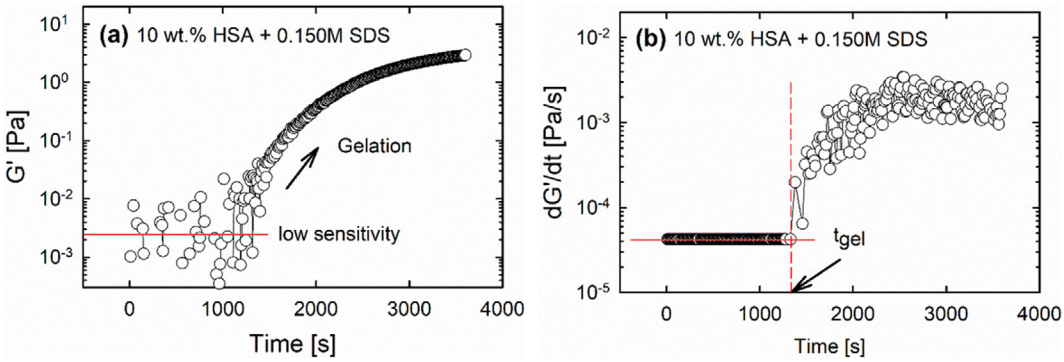

Fig. 5. (a) A typical gelation curve for 10 wt% HSA with 0.150 M SDS. (b) t_{gel} was observed as the first change in the derivative of G′ for 10 wt% HSA with 0.150 M SDS. Averaged values are used in the low-sensitivity region because G′ values fluctuate before gelation when the measured torque is close to rheometer sensitivity.

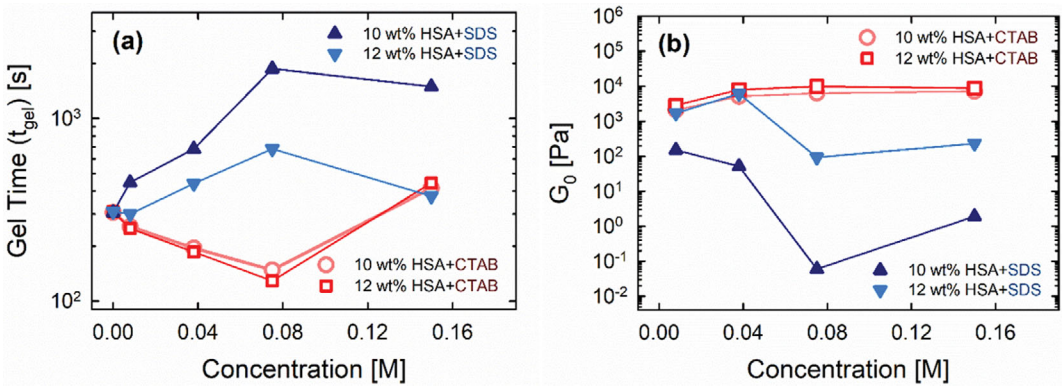

Fig. 6. (a) Variation in t_{gel} of 10 and 12 wt% HSA with CTAB or SDS as a function of concentration; (b) Variation in plateau modulus (G_0) of 10 and 12 wt% HSA with CTAB or SDS as a function of concentration.

than HSA/SDS gels and exhibit increasing synaeresis at high CTAB concentrations. Interestingly, other proteins exhibit synaeresis at low pH [11].

While the trends of both the isothermal and nonisothermal gelation kinetics agreed, the elastic moduli at the end of the gelation plateau for both kinetics differed. The plateau modulus measured under isothermal conditions for both CTAB and SDS was higher than that under nonisothermal conditions. This may be due to the greater amount of thermal energy delivered under isothermal conditions than under nonisothermal conditions.

To elucidate the effects of both surfactants on the isothermal gelation behavior of HSA, the gelation time (t_{gel}) for 10 and 12 wt% HSA in CTAB or SDS was calculated by observing the first change in the time derivative of G′. Representative determination for wt% HSA with 0.150 M SDS is illustrated in Fig. 5(b). To compare the effect of CTAB and SDS concentration on the t_{gel} of HSA, the plots of the obtained t_{gel} are shown in Fig. 6(a). Increasing the CTAB concentration up to 0.08 M reduced the t_{gel} of HSA/CTAB, whereas increasing the concentration to 0.150 M resulted in a trend reversal and increment in t_{gel} to more than that of the pure protein. In contrast, increasing the SDS concentration to up to 0.08 M increased t_{gel}. However, at an SDS concentration of 0.150 M, t_{gel} decreased. Increasing the concentration of HSA appears to have a less significant effect on the t_{gel} of HSA/CTAB than HSA/SDS, and a similar insignificant effect is also observed at higher HSA concentration under nonisothermal conditions (7 and 10 wt%), whereas it resulted to a significant decrease in t_{gel} with SDS.

The plateau modulus attained during the gelation process depends on the number of protein crosslinks formed. The plateau modulus calculated by fitting the time sweep data to the Boltzmann sigmoidal function is depicted in Fig. 6(b). Details of the model and fitted curves are contained in Supporting Information (Fig. S4). HSA with CTAB exhibited high-level crosslinking with less dependence on the protein concentration compared with HSA in SDS. The crosslinking level of HSA in SDS hydrogels diminished significantly beyond 0.038 M and exhibited considerable variation with the protein concentration, observed as a significant difference between the plateau modulus values for 10 and 12 wt% HSA with SDS.

4. Frequency Sweep Testing of HSA/CTAB and HSA/SDS Gels

The frequency sweep results of 10 and 12 wt% HSA in CTAB or SDS are plotted in Fig. 7(a)-(d). HSA/CTAB displays characteristic solid material response (G′>>G″). Both G′ and G″ are nearly flat and frequency-independent across the covered frequency range. Furthermore, both G′ and G″ are stable or increased but not diminished across the covered CTAB concentrations, indicating mechanically stable gels. However, HSA/SDS gels exhibited solid gel-like behavior at lower (<0.038 M) SDS concentrations; however, beyond

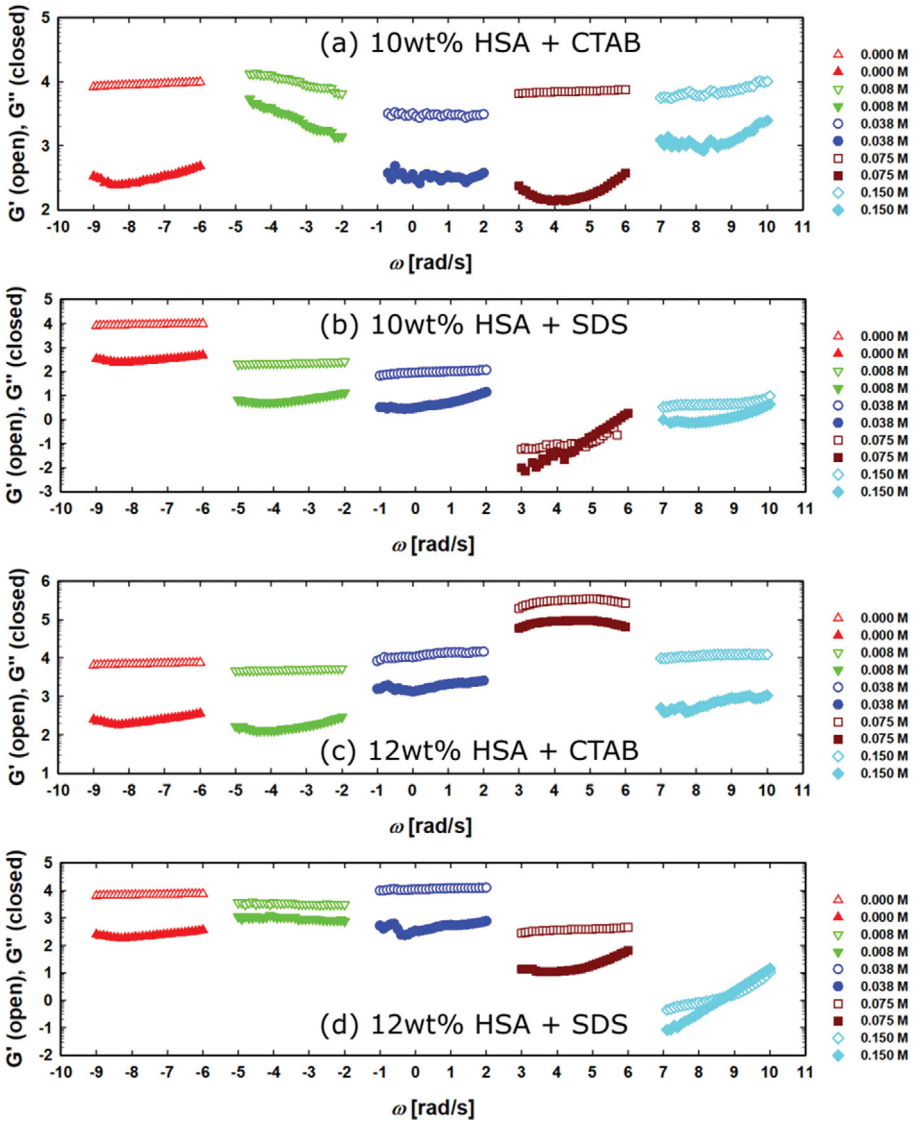

Fig. 7. (a) Variation in G′ and G″ with frequency over surfactant concentrations 0-0.15 M for (a) 10 wt% HSA with CTAB, (b) 10 wt% HSA with SDS, (c) 12 wt% HSA with CTAB, and (d) 12 wt% HSA with SDS.

0.038 M surfactant concentration, G′ and G″ exhibited diminished response at both 10 and 12 wt% HSA. At an SDS concentration of 0.075 M with 10 wt% HSA or 0.150 M with 12 wt% HSA, the resultant gel exhibited frequency-responsive behavior in terms of G′ and G″, with G′>G″ at low frequency, a cross-over, and G″>G′ at high frequency. Overall, HSA/CTAB exhibited the least variability in mechanical property over the entire frequency and surfactant concentration range compared with HSA/SDS.

5. Molecular Level Rationalization of Fast HSA/CTAB and Slow HSA/SDS Gelation Kinetics

MD simulation was employed to elucidate the interaction between HSA and either surfactant at a molecular level because the viscoelastic evolution associated with the sol-gel transition of protein solutions originating from molecular level changes in noncovalent interactions such as electrostatic, hydrogen bonding, and hydrophobic interaction between protein molecules [37]. The effect of either surfactant on the evolution of the HSA structure was investigated by estimating the number of alpha-helical structures retained at the end of the simulation run. The native HSA secondary structure is predominantly alpha-helical; therefore, the helicity estimation provides a reasonable measure of the unfolding level of proteins and thus may be used to assess the likelihood of aggregation and gelation. A more unfolded HSA structure exposes more hydrophobic sites that drive aggregation through hydrophobic association [52] and increases the protein dimensions, reducing the energy barrier to aggregation.

The structure of HSA from the end frame of the MD simulation was used to perform this calculation. The calculation was performed using the stride server [53], and the results are shown in Fig. 8(a). The results show a greater loss of the helical structure of HSA in HSA/CTAB mixtures than that of HSA/SDS, indicating greater unfolding and thus higher aggregation propensity in the former, which agrees well with our experimental findings. The estimated helicity agrees qualitatively with that recently obtained experi-

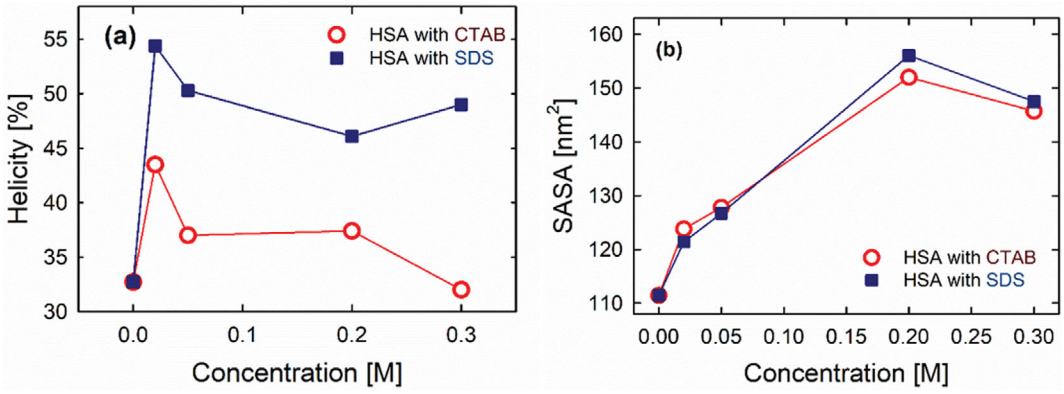

Fig. 8. Estimated (a) helicity of HSA and (b) SASA obtained from MD simulation trajectories after 150 ns.

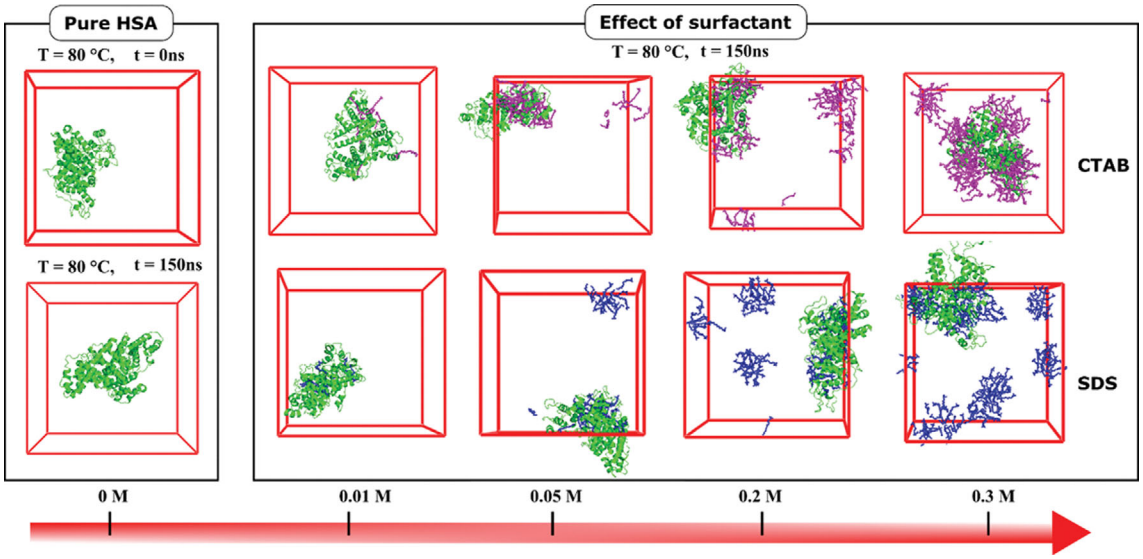

Fig. 9. Secondary structure of HSA showing the helix in green at t=0 (i.e., the initial structure of HSA), and after 150-ns simulation without surfactant, followed by 150-ns simulation in the presence of CTAB (pink) or SDS (blue) at 150 ns.

mentally for HSA containing varying SDS concentration [45]. A quantitative agreement has not been achieved with MD simulation due to underestimation or overestimation of helicity resulting from force field bias [54-56]. Without a surfactant, the helicity of HSA decreased as the protein unfolded, from its initial value of 67% to 34% after 150 ns. Overall, the result showed that CTAB effected greater loss of helical structure on HSA than SDS over the concentrations covered by MD simulation.

The interaction of the surfactants and the greater loss of HSA helicity in CTAB than in SDS are illustrated by the snapshot of the protein initial structure and the structure after 150 ns in various surfactant concentrations in Figs. 9 and 10. These figures reveal changes in the interaction between the protein and surfactant (CTAB and SDS) molecules at low and high surfactant concentration regimes. Comparatively, CTAB bound more with HSA than SDS. The greater binding of CTAB than SDS can be attributed to the less repulsive interaction between HSA and CTAB in comparison to HSA and SDS, as determined through net charge calculations (refer to Tables S4 and S5 in the supporting information). As the concentration of CTAB increased, HSA's absolute net charge initially decreased until it reached its lowest point near 0.038 M, after which it reversed. Conversely, the addition of SDS increased HSA's absolute net charge, resulting in greater electrostatic repulsion, which inhibited further binding. The solvent accessible area (SASA) is considered a decisive factor for estimating the protein fold state [27,56]. Higher SASA values suggest greater protein denaturation. The SASA of the HSA structure was calculated from the MD trajectory and plotted in Fig. 8(b). The obtained SASA values indicate that HSA denaturation increases with increasing concentration of both CTAB and SDS surfactants until it reaches a maximum at 0.2 M (surfactant/protein molar ratio of 100) and then decreases.

Furthermore, a comparison of the radial distribution function of CTAB and SDS from the protein surface at all concentrations, as plotted in Fig. 11(a)-(d), strongly supports the existence of stronger HSA-CTAB interaction than HSA-SDS. This is evidenced by considerably higher peaks for CTAB than SDS near the protein surface [57]. The greater distribution of CTAB close to the protein surface affirms the depletion of HSA hydration water with increasing

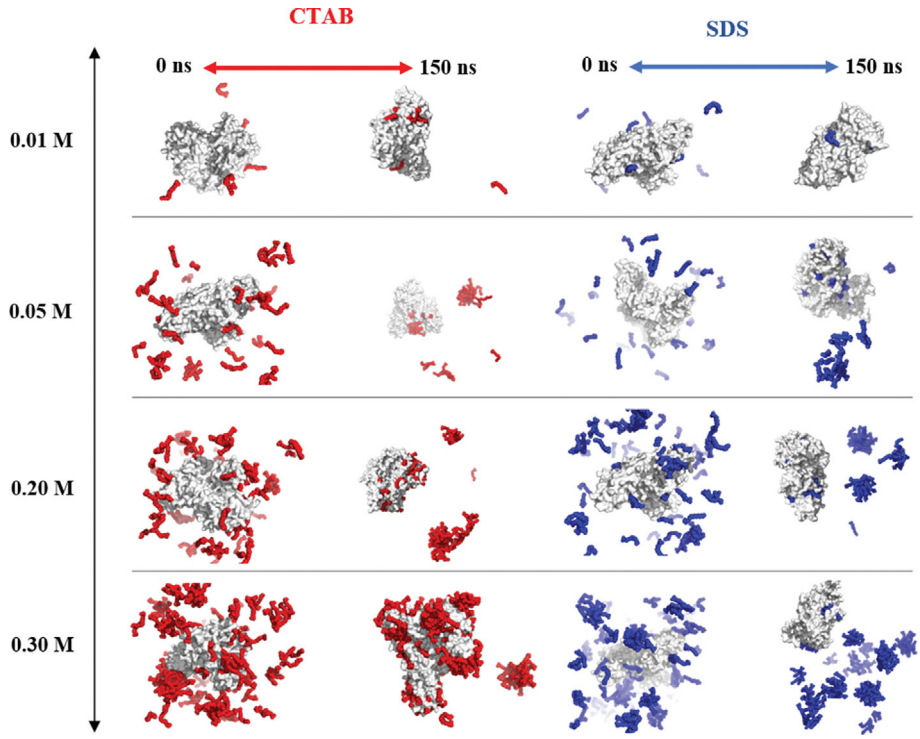

Fig. 10. Snapshots showing the molecular configuration at 0 and 150 ns of MD simulation for HSA (white surface) with CTAB (red spheres) and SDS (blue spheres) at various concentrations.

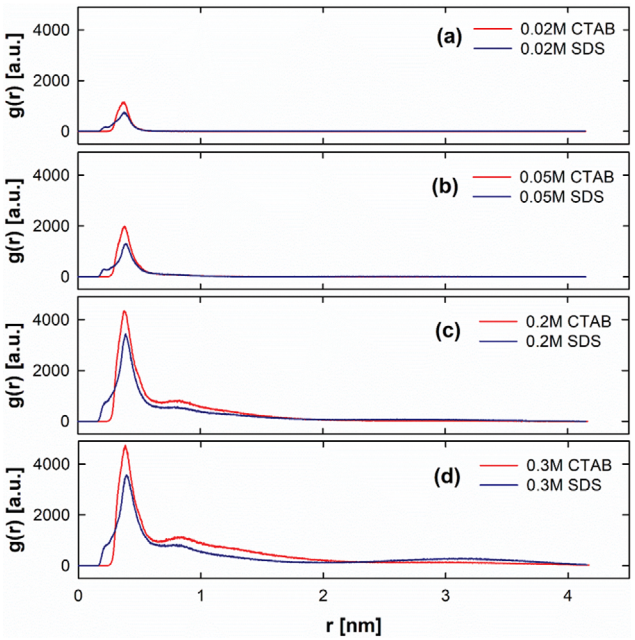

Fig. 11. Radial distribution functions, g(r), of CTAB and SDS from the HSA surface at (a) 0.02 M, (b) 0.05 M, (c) 0.2 M, and (d) 0.3 M.

CTAB concentration. The closer distribution of CTAB to HSA than SDS is due to the stronger electrostatic interaction of CTAB with charged groups on the protein surface, which outcompetes water molecules [58]. Due to the net charge differences, CTAB binding to HSA is expected to lower the long-range protein-protein repulsive interaction, which otherwise prevents the protein from aggregation [27].

CONCLUSION

The effects of increasing the concentration of singly charged CTAB or SDS surfactants on the gelation dynamics of HSA were investigated by rheological methods of temperature ramping and time sweep testing. Under temperature ramp conditions (nonisothermal conditions), the T_{gel} (gelation temperature) of HSA/CTAB solutions decreased relative to that of HSA as the CTAB concentration increased. However, at higher CTAB concentration, the T_{gel} of HSA/CTAB solutions reversed the trend and began to increase with CTAB concentration, probably because of an increase in CTAB-CTAB interaction as opposed to more profound HSA/CTAB at low CTAB concentration. In contrast, increasing SDS concentrations gradually increased the T_{gel} of HSA/SDS solutions at low SDS concentration, following rising repulsive interaction among HSA/SDS complexes corresponding to an increment in the energy barrier toward aggregation. Nonisothermal kinetics revealed a first-order gelation process for HSA in both surfactants, with CTAB addition producing complexes with lowered activation energy, whereas SDS addition is marked with increasing activation energy.

Under time sweep conditions (isothermal conditions, temperature at 80 °C), increasing CTAB concentration reduced the t_{gel} of HSA/CTAB solutions, and similar to the results from the temperature ramp tests, the trend reversed at high CTAB concentration. Conversely, HSA/SDS solutions exhibited decreased t_{gel} as the SDS

concentration increased but exhibited a minor decrease at the maximum SDS concentration measured. Overall, the protein concentration did not affect the t_{gel} of HSA/CTAB, but its effect on HSA/SDS was significant, with an increase in HSA concentration increasing the t_{gel} of HSA/SDS.

The MD simulation results revealed a faster unfolding of HSA helices with increasing CTAB concentration at 80 °C, which is more favorable for the aggregation of HSA in HSA/CTAB aqueous solutions than in HSA/SDS aqueous solutions, resulting in a lower gelation temperature and gelation time of HSA/CTAB, as seen in the temperature ramp and time sweep results. Visual analysis of snapshots from the beginning and end of the MD simulation showed different aggregation behavior of the surfactants at low and high concentration. At low concentration, the molecules of both surfactants are attracted closely to HSA. However, at higher surfactant concentration, surfactant-surfactant aggregation predominates the simulation box. Comparatively, CTAB interacted with HSA more than SDS at all concentrations. These findings are useful for understanding protein-surfactant viscoelasticity for industrial applications.

ACKNOWLEDGEMENTS

This research was supported by the National Research Foundation of Korea (NRF) grant funded by the Korea government (No. 2021R1I1A3054572).

COMPETING INTERESTS

The authors declare that they have no known competing financial interests or personal relationships that could have appeared to influence the work reported in this paper.

SUPPORTING INFORMATION

Additional information as noted in the text. This information is available via the Internet at http://www.springer.com/chemistry/journal/11814.

REFERENCES

1. M. Fasano, S. Curry, E. Terreno, M. Galliano, G. Fanali, P. Narciso, S. Notari and P. Ascenzi, *IUBMB Life (International Union of Biochemistry and Molecular Biology: Life)*, **57**, 787 (2005).
2. R. Panahi and M. Baghban-Salehi, *Polym. Polym. Compos.: A Ref. Ser.*, 1561 (2019).
3. P. Hájovská, M. Chytil and M. Kalina, *Int. J. Biol. Macromol.*, **161**, 738 (2020).
4. A. Oliva, A. Santoveña, M. Llabres and J. B. Fariña, *J. Pharm. Pharmacol.*, **51**, 385 (1999).
5. J. Park, M.-S. Kim, T. Park, Y. H. Kim and D. H. Shin, *Int. J. Biol. Macromol.*, **166**, 221 (2021).
6. A. Hashem, C. O. Aniagor, M. A. F. Afifi, A. Abou-Okeil and S. H. Samaha, *Korean J. Chem. Eng.*, **38**, 2157 (2021).
7. S. K. Seidlits, Z. Z. Khaing, R. R. Petersen, J. D. Nickels, J. E. Vanscoy, J. B. Shear and C. E. Schmidt, *Biomaterials*, **31**, 3930 (2010).
8. S. Lim, D. Jeong, M.-R. Ki, S. P. Pack and Y. S. Choi, *Korean J. Chem. Eng.*, **38**, 98 (2021).
9. C. Yan and D. J. Pochan, *Chem. Soc. Rev.*, **39**, 3528 (2010).
10. O. S. Nnyigide and K. Hyun, *Rheol. Acta*, **57**, 563 (2018).
11. A. Aufderhorst-Roberts, M. D. Hughes, A. Hare, D. A. Head, N. Kapur, D. J. Brockwell and L. Dougan, *Biomacromolecules*, **21**, 4253 (2020).
12. K. Hyun, M. Wilhelm, C. O. Klein, K. S. Cho, J. G. Nam, K. H. Ahn, S. J. Lee, R. H. Ewoldt and G. H. McKinley, *Prog. Polym. Sci.*, **36**, 1697 (2011).
13. L. Böcker, P. A. Rühs, L. Böni, P. Fischer and S. Kuster, *ACS Biomater. Sci. Eng.*, **2**, 90 (2015).
14. L. Liu, J. You, H. Zhu and W. Tan, *Korean J. Chem. Eng.*, **39**, 1927 (2022).
15. O. S. Nnyigide and K. Hyun, *Korean J. Chem. Eng.*, **35**, 1969 (2018).
16. O. S. Nnyigide, T. O. Nnyigide and K. Hyun, *Carbohydr. Polym.*, **251**, 117061 (2021).
17. Q. Yuan, X. Lu, K. H. Khayat, D. Feys and C. Shi, *Mater. Struct.*, **50**, 112 (2016).
18. M. Kim and K. Hyun, *Korea-Aust. Rheol. J.*, **33**, 25 (2021).
19. S. H. Lee, S. Y. Kim, R. Salehiyan and K. Hyun, *Korea-Aust. Rheol. J.*, **33**, 321 (2021).
20. J. W. Rhim, R. V. Nunes, V. A. Jones and K. R. Swartzel, *J. Food Sci.*, **54**, 446 (1989).
21. J.-T. Fu and M. A. Rao, *Food Hydrocolloids*, **15**, 93 (2001).
22. S. A. Madbouly and J. U. Otaigbe, *Macromolecules*, **39**, 4144 (2006).
23. J. Jezek, M. Rides, B. Derham, J. Moore, E. Cerasoli, R. Simler and B. Perez-Ramirez, *Adv. Drug Deliv. Rev.*, **63**, 1107 (2011).
24. W. J. Galush, L. N. Le and J. M. R. Moore, *J. Pharm. Sci.*, **101**, 1012 (2012).
25. J. H. Gu, R. Qian, R. Chou, P. V. Bondarenko and M. Goldenberg, *Pharm. Res.*, **35**, (2018).
26. J. A. Lemkul, W. J. Allen and D. R. Bevan, *J. Chem. Inf. Model.*, **50**, 2221 (2010).
27. O. S. Nnyigide and K. Hyun, *J. Biomolec. Struct. Dynamics*, **39**, 1106 (2020).
28. O. S. Nnyigide and K. Hyun, *Food Hydrocolloids*, **103**, 105656 (2020).
29. S. Sugio, A. Kashima, S. Mochizuki, M. Noda and K. Kobayashi, *Protein Eng., Des. Selection*, **12**, 439 (1999).
30. S. Sugio, A. Kashima, S. Mochizuki, M. Noda and K. Kobayashi, RCSB PDB:1AO6 (1998).
31. C. Oostenbrink, A. Villa, A. E. Mark and W. F. Van Gunsteren, *J. Comput. Chem.*, **25**, 1656 (2004).
32. G. Petekidis, *J. Rheol.*, **58**, 1085 (2014).
33. M. C. Childers and V. Daggett, *J. Phys. Chem. B*, **122**, 6673 (2018).
34. K. A. Dill and J. L. MacCallum, *Science*, **338**, 1042 (2012).
35. E. Jacob and R. Unger, *Bioinformatics*, **23**, e225 (2007).
36. A. W. Senior, R. Evans, J. Jumper, J. Kirkpatrick, L. Sifre, T. Green, C. Qin, A. Žídek, A. W. Nelson, A. Bridgland, H. Penedones, S. Petersen, K. Simonyan, S. Crossan, P. Kohli, D. T. Jones, D. Silver, K. Kavukcuoglu and D. Hassabis, *Nature*, **577**, 706 (2020).
37. S. H. Arabi, B. Aghelnejad, C. Schwieger, A. Meister, A. Kerth and D. Hinderberger, *Biomater. Sci.*, **6**, 478 (2018).
38. C. Le Bon, T. Nicolai and D. Durand, *Macromolecules*, **32**, 6120 (1999).
39. T. Nicolai, *Adv. Colloid Interface Sci.*, **270**, 147 (2019).
40. T. K. Vo, S.-S. Kim and J. Kim, *Korean J. Chem. Eng.*, **39**, 1478 (2022).

41. P. R. Avallone, E. Raccone, S. Costanzo, M. Delmonte, A. Sarrica, R. Pasquino and N. Grizzuti, *Food Hydrocolloids*, **111**, 106248 (2021).
42. P. H. Santos, O. H. Campanella and M. A. Carignano, *J. Phys. Chem. B*, **114**, 13052 (2010).
43. O. S. Nnyigide, Y. Oh, H. Y. Song, E.-k. Park, S.-H. Choi and K. Hyun, *Korea-Aust. Rheol. J.*, **29**, 101 (2017).
44. V. Normand, S. Muller, J.-C. Ravey and A. Parker, *Macromolecules*, **33**, 1063 (2000).
45. Y. Moriyama and K. Takeda, *J. Oleo Sci.*, **66**, 521 (2017).
46. N. Fogh-Andersen, P. J. Bjerrum, and O. Siggaard-Andersen, *Clin. Chem.*, **39**, 48 (1993).
47. M. Javed, S. Iqbal, I. Fatima, S. Nadeem, A. Mohyuddin, M. Arif, A. Amjad, S. Shahid, F. H. Alshammari, M. I. Alahmdi, E. B. Elkaeed, R. M. Alzhrani, N. S. Awwad, H. A. Ibrahium and M. A. Qayyum, *Colloid Interface Sci. Commun.*, **48**, 100623 (2022).
48. P. Sandkühler, J. Sefcik and M. Morbidelli, *Langmuir*, **21**, 2062 (2005).
49. W. Wang, *Int. J. Pharm.*, **289**, 1 (2005).
50. T. Zlateva, R. Boteva, B. Salvato and R. Tsanev, *Int. J. Biol. Macromol.*, **26**, 357 (1999).
51. J. A. L. da Silva, M. P. Gonçalves and M. A. Rao, *Int. J. Biol. Macromol.*, **17**, 25 (1995).
52. A. Stenstam, A. Khan and H. Wennerström, *Langmuir*, **17**, 7513 (2001).
53. M. Heinig and D. Frishman, *Nucleic Acids Res.*, **32**, 500 (2004).
54. Z. Cao and J. Wang, *J. Biomolec. Struct. Dynamics*, **27**, 651 (2010).
55. K. K. Patapati and N. M. Glykos, *PLoS ONE*, **5**, e15290 (2010).
56. J. F. Zayas, *Functionality of proteins in food*, Springer Berlin (2013).
57. O. S. Nnyigide, S.-G. Lee and K. Hyun, *Sci. Rep.*, **9**, 10643 (2019).
58. O. S. Nnyigide, S.-G. Lee and K. Hyun, *J. Mol. Model.*, **24**, 1 (2018).

Supporting Information

Rheological and molecular dynamics simulation studies of the gelation of human serum albumin in anionic and cationic surfactants

Tochukwu Olunna Nnyigide, Osita Sunday Nnyigide, and Kyu Hyun[†]

School of Chemical Engineering, Pusan National University, Busan 46241, Korea
(*Received 23 April 2023 • Revised 12 June 2023 • Accepted 14 June 2023*)

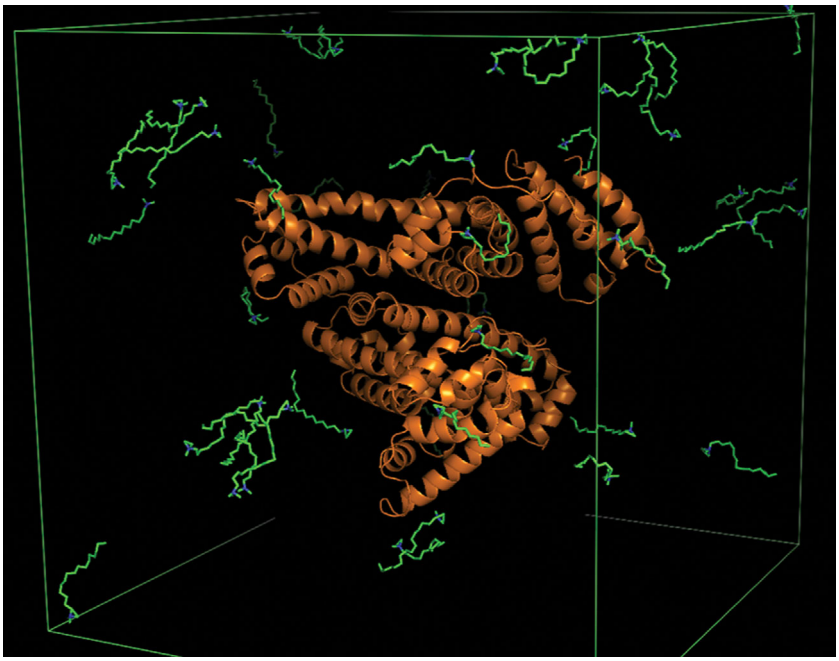

Fig. S1. Simulation box of HSA in 0.05 M CTAB. Cartoon structure of HSA is shown in orange and ball/stick representation of CTAB is shown in CPK colors with. Water molecules and counter ions are hidden for brevity.

Table S1. Contents of HSA/CTAB solution[a] simulation box

CTAB [M]	N_{water}	N_{CTAB}
0.00	43897	0
0.01	43801	8
0.05	43335	42
0.20	42792	165
0.30	41685	248

Table S2. Contents of HSA/SDS solution[b] simulation box

SDS [M]	N_{water}	N_{SDS}
0.00	43897	0
0.01	43801	8
0.05	43335	42
0.20	42792	165
0.30	41685	248

Table S3. Comparison of average molar ratios of surfactant in experiment (10 wt% HSA) and simulation

Experiment surfactant concentration [M]	Simulation concentration [M]	Surfactant/HSA molar ratio [-]
0.000	0	0
0.008	0.01	5
0.038	0.05	25
0.075	0.20	100
0.150	0.30	150

Table S4. Calculated average net charge per HSA molecule (C^*_{CTAB}) at different CTAB concentrations

CTAB [M]	C^*_{CTAB} [HSA=5 wt%]	C^*_{CTAB} [HSA=7 wt%]	C^*_{CTAB} [HSA=10 wt%]
0.000	−24.00	−24.00	−24.00
0.008	−13.885	−16.927	−19.209
0.038	+24.578	+9.939	−1.010
0.075	+73.205	+43.969	+22.045
0.150	+176.036	+115.866	+70.752

Table S5. Calculated average net charge per HSA molecule (C^*_{SDS}) at different SDS concentrations

SDS [M]	C^*_{SDS} [HSA=5 wt%]	C^*_{SDS} [HSA=7 wt%]	C^*_{SDS} [HSA=10 wt%]
0.000	−24.00	−24.00	−24.00
0.008	−34.085	−31.052	−28.777
0.038	−71.903	−57.496	−46.691
0.075	−118.546	−90.111	−68.785
0.150	−213.092	−156.222	−113.570

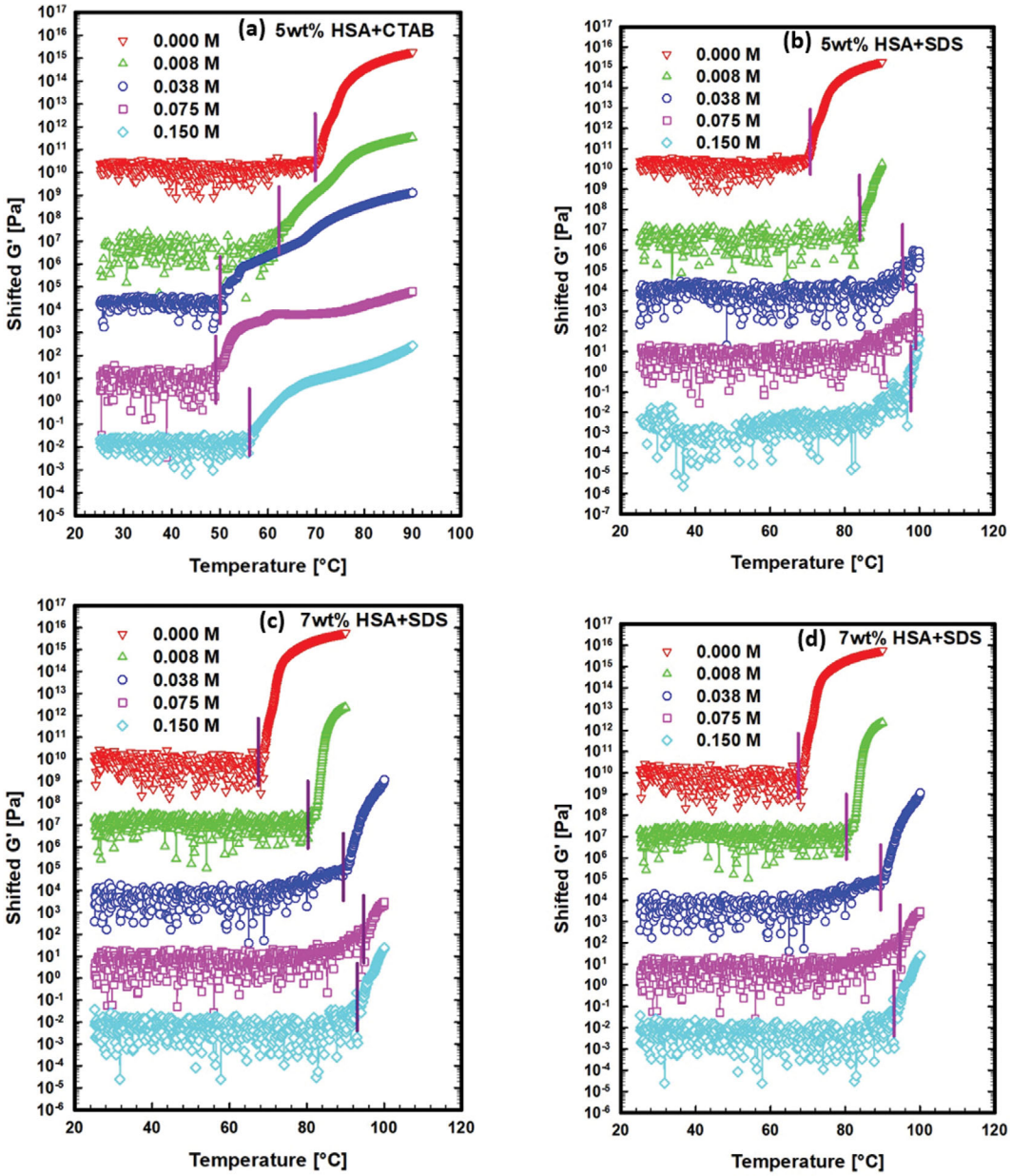

Fig. S2. (a)-(f) Temperature ramp results of 5, 7, 10 wt% HSA in different CTAB/SDS concentrations.

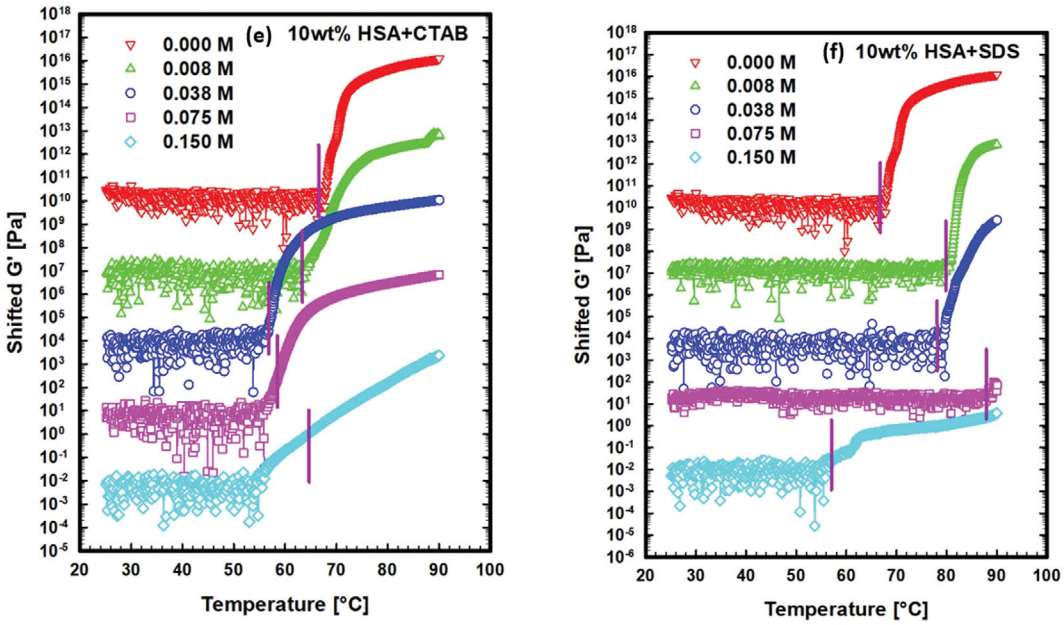

Fig. S2. Continued.

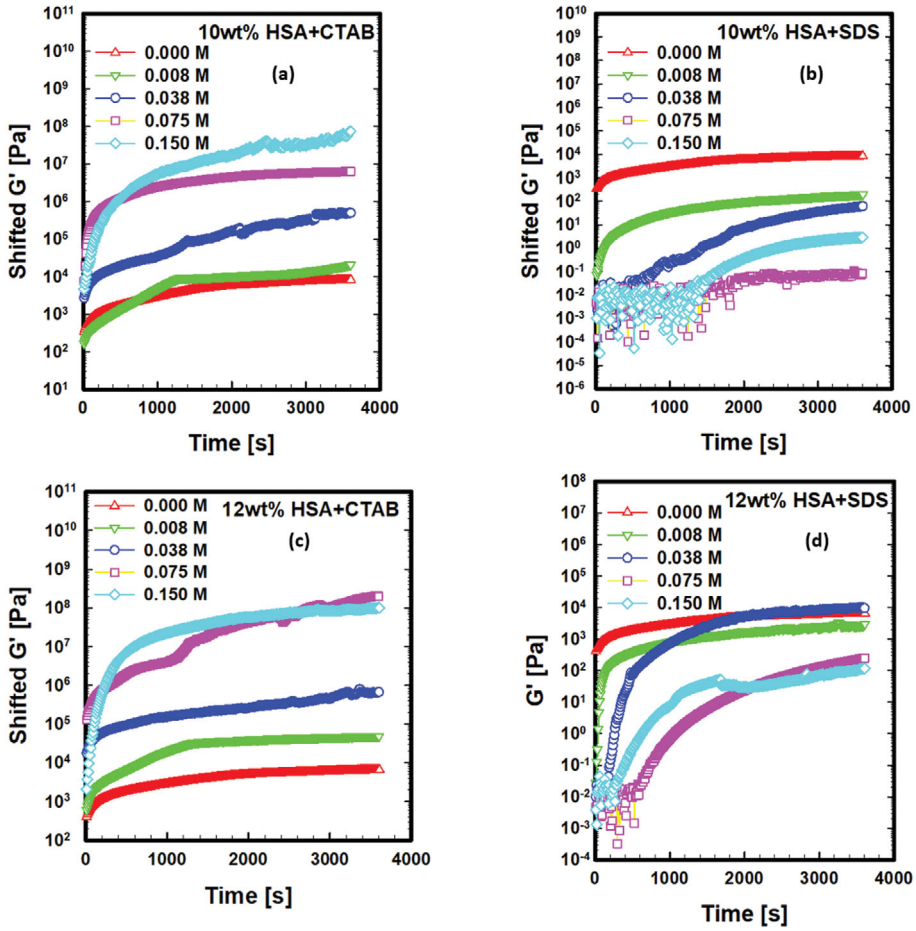

Fig. S3(a)-(d) Time sweeps of 10 and 12 wt% in different CTAB/SDS concentrations.

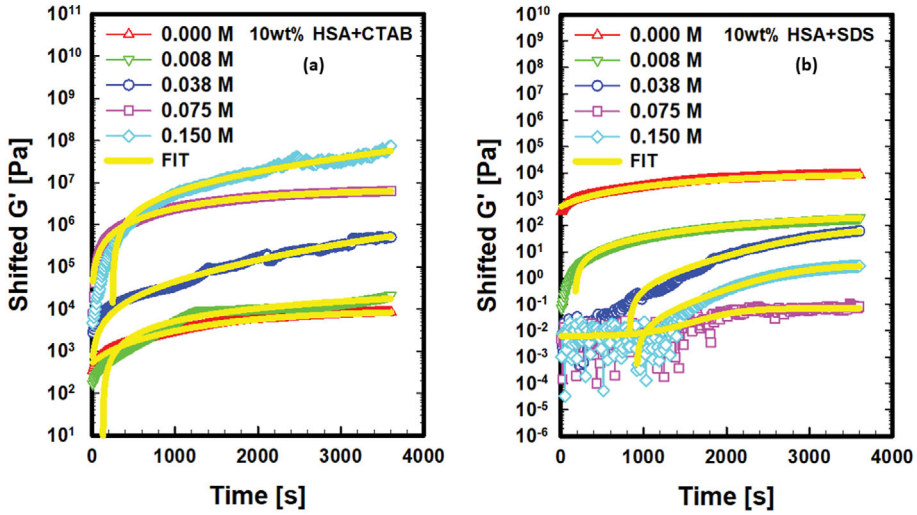

Fig. S4. (a)-(b) Fitting for the determination of plateau modulus G^0.